Spatial and temporal variability of N_2O emissions in a subtropical forest catchment in China

Running title: N_2O emissions in subtropical China

Author: Zhu J.[1], Mulder J.[1], Wu L.P.[2], Meng X.X.[2], Wang Y.H.[3] and Dörsch P.[1]

Affiliation:

[1] Norwegian University of Life Sciences, postbox 5003, Ås-1432, Norway

[2] Chongqing Academy of Environmental Sciences and Monitoring, Qishan Road 252, Chongqing, China

[3] Institute of Forest Ecology, Environment and Protection, Chinese Academy of Forestry, Wan-Shou-Shan, Beijing, 100091, China

Corresponding author:

J. Zhu, tel.: +47 6496 6218, fax: +47 6496 5601, e-mail: jing.zhu@umb.no

Keywords:

Nitrous oxide (N_2O), subtropical, forest, catchment, TieShanPing (TSP), water filled pore space (WFPS), soil temperature

Paper type: primary research articles

Abstract

Subtropical forests in South China have received chronically large amounts of atmogenic nitrogen (N) causing N saturation. Recent studies suggest that a significant proportion of the N input is returned to the atmosphere, in part as nitrous oxide (N_2O). We measured N_2O emission fluxes by closed chamber technique throughout two years in a Masson pine-dominated headwater catchment with acrisols (pH~4) at TieShanPing (Chongqing, SW China) and assessed the spatial and temporal variability in two landscape elements typical for this region: a mesic forested hill slope (HS) and a hydrologically connected, terraced groundwater discharge zone (GDZ) in the valley bottom. High emission rates of up to 1800 µg N_2O-N m^{-2} hr^{-1} were recorded on the HS shortly after rain storms during monsoonal summer, whereas emission fluxes during the dry winter season were generally low. Overall, N_2O emission was lower in GDZ than in HS, rendering the mesic HS the dominant source of N_2O in this landscape. Temporal variability of N_2O emissions on HS was largely explained by soil temperature and moisture, pointing at denitrification as a major process for N removal and N_2O production. The concentration of nitrate (NO_3^-) in pore water on HS was high even in the rainy season, apparently never limiting denitrification and N_2O production. The concentration of NO_3^- decreased along the terraced GDZ, indicating efficient N removal, but with moderate N_2O-N loss. The extrapolated annual N_2O fluxes from soils on HS (0.54 and 0.43 g N_2O-N m^{-2} yr^{-1} for a year with a wet and a dry summer, respectively) are among the highest N_2O fluxes

41 reported from subtropical forests so far. Annual N_2O-N emissions amounted to 8-10%
42 of the annual atmogenic N deposition, suggesting that forests on acid soils in South
43 China are an important, hitherto overlooked component of the anthropogenic N_2O
44 budget.

1. Introduction

The global atmospheric concentration of nitrous oxide (N_2O), an important greenhouse gas and decomposer of stratospheric ozone, has increased from a pre-industrial level of 270 ppbv to 322 ppbv in 2008 (WMO, 2009). The global source strength is estimated to be 17.7 Tg N yr^{-1}, with agriculture contributing 2.8 (1.7-4.8) Tg N yr^{-1} and soils under natural vegetation 6.6 (3.3-9.0) Tg N yr^{-1} (IPCC, 2007; Hirsch et al., 2006). Both, estimates based on bottom-up approaches (Stehfest and Bouwman, 2006) and on observations of the N_2O atmospheric column (Kort et al., 2011; D'Amelio et al., 2009; Hirsch et al., 2006) suggest that 50-64% of the atmospheric N_2O derive from the (sub)tropical zone 0^o to 30^oN. Much of the N_2O attributable to this zone is emitted from forest soils (Melillo et al., 2001; Werner et al., 2007a; Rowlings et al., 2012). So far, N_2O flux data from subtropical forests are scarce making this biome an under-investigated component of the global N_2O budget.

Large parts of southern China are situated in the humid subtropics and the dominant forest types are evergreen broadleaf and coniferous forest, many of which are found as patches in densely populated areas with intensive agriculture. Due to strong increases in the emission of nitrogen oxides (NO_x) and ammonia (NH_x), caused by combustion of fossil fuels and massive fertilizer use, respectively (Xiong et al., 2008; Liu et al., 2011b), these forests receive high amounts of reactive nitrogen (N_r) by atmogenic deposition, mostly as ammonium (NH_4^+). A recent study of five forested

65 watersheds in South China found various degrees of N saturation (Chen and Mulder,
66 2007a), i.e. rates of atmogenic N_r input exceeding uptake by vegetation (Aber et al.,
67 2003) and causing elevated concentrations of nitrate (NO_3^-) in the root zone. Larssen
68 et al. (2011) reported moderate NO_3^- export with stream water in these watersheds,
69 despite low forest productivity, suggesting major unaccounted N sinks in these
70 ecosystems.

71 One possible fate of excess N may be gaseous emission as nitric oxide (NO), N_2O or
72 dinitrogen (N_2) produced during nitrification and denitrification. Known factors
73 controlling N_2O emissions are availability of inorganic N and degradable organic
74 carbon (C), soil temperature, soil moisture and soil pH (Parton et al., 1996; Flessa et
75 al., 1995; Smith et al., 2003; Weier et al., 1993; Simek and Cooper, 2002). The
76 monsoonal climate in South China provides favorable conditions for both nitrification
77 and denitrification as much of the annual N input, dominated by NH_4^+, occurs during
78 rain storms in summer when soils are warm and N turnover rates high. Moreover,
79 forests in South China are often found on acidic soils. Acidity has been reported to
80 support high N_2O/N_2 product ratios in denitrification (Liu et al., 2010b; Bergaust et al.,
81 2010) which could result in high N_2O emissions. Acidity also inhibits autotrophic
82 nitrification by reducing the availability of ammonia (NH_3), the actual substrate for
83 membrane-bound ammonia mono-oxygenase in ammonia oxidizing bacteria (De Boer
84 and Kowalchuk 2001); on the other hand, low soil pH may enhance the apparent N_2O
85 yield of nitrification, possibly involving chemodenitrification of nitrite (NO_2^-) from

either nitrification or dissimilatory NO_2^- reduction (Mørkved et al. 2007). Therefore the net effect of acidity on the production of nitrification-related N_2O is still uncertain.

Few studies have addressed N_2O emissions in Chinese subtropical forests. Tang et al. (2006) studied the temporal variation of N_2O fluxes in a pine, a mixed and an evergreen broadleaf forest on acid soils in the Dinghushan catchment, South China throughout one year and found highest emissions during the wet-hot season. Based on weekly to biweekly measurements, they estimated an annual emission of 3.2 kg N_2O-N ha^{-1} which is above the reported average N_2O emission of 1.2–1.4 kg N ha^{-1} yr^{-1} for tropical forests (Stehfest and Bouwman, 2006; Werner et al., 2007b). Fang et al. (2009) reported 2.0 to 2.4 kg N_2O-N loss ha^{-1} yr^{-1} based on monthly measurements along a hillslope in an evergreen broadleaf forest in the same catchment. Lin et al. (2010; 2012) estimated smaller average annual N_2O emissions of 0.13 and 0.71 kg N ha^{-1} for pine forests in Hubei province, probably due to the higher pH of these forest soils.

Estimates of annual N_2O emissions in forested catchments are fraught by large temporal and spatial variability commonly reported for N_2O fluxes. Forests in subtropical China are typically found on sloping terrain and mountain ridges, resulting in hydrological gradients known to affect N_2O emissions. For example, Fang et al. (2009) found that N_2O emissions increased with soil moisture from hilltop to the bottom of a hill slope. Besides soil moisture, other soil factors, such as pH, texture,

106 vegetation type and productivity may vary along hydrological flow paths, resulting in
107 distinct spatial patterns of N_2O emissions (Osaka et al., 2006; Lark et al., 2004).
108 Ultimately, soil factors related to topography may shape distinct nitrifier and
109 denitrifier communities with respect to N_2O turnover (Philippot et al., 2009; Dörsch et
110 al., 2012; Wessen et al., 2011; Banerjee and Siciliano, 2012). Thus, understanding of
111 spatial and temporal variability of N_2O emission fluxes and their drivers on a
112 landscape level are indispensable for improving regional estimates of N_2O emissions.

113 The objective of the present study was to estimate N_2O fluxes in an N-saturated
114 forested catchment in Southwest China and to explore their main drivers in space and
115 time. More specifically, we investigated the seasonal distribution of emission fluxes
116 (dry versus wet season), the role of storm flow conditions on peak N_2O emissions and
117 the spatial distribution of N_2O emissions along a hydrological flow path on a hill
118 slope (HS) and a groundwater discharge zone (GDZ). We hypothesized that the
119 emission strength is higher during the wet season than the dry season and that a
120 substantial part of the annual N_2O emission occurs during transient N_2O emission
121 peaks triggered by rain episodes. In addition, based on previous observations that the
122 water-saturated GDZ has large N retention (Larssen et al. 2011), we hypothesized the
123 GDZ to act as a zone of increased denitrification and hence high N_2O emission
124 relative to the well-drained HS. Emissions of N_2O were measured together with soil
125 parameters from summer 2009 to autumn 2010, along two transects in each of the two
126 landscape elements, hillslope (HS) and ground water discharge zone (GDZ). To

improve flux estimates in time, a regression model is proposed interpolating temporally discrete N_2O measurements on the HS based on continuously recorded soil moisture and temperature.

2. Materials and methods

2.1 Site description

The Tieshanping (TSP) catchment is a 16.2 ha headwater catchment, 450 m asl, located on a forested ridge about 25 km Northeast of Chongqing city, SW China (29°38'N 104°41'E, Fig. 1a). Details on climate, vegetation and soil characteristics as well as atmogenic N deposition can be found elsewhere (Chen and Mulder, 2007a). The area has a typical subtropical monsoonal climate with a mean annual precipitation of 1028 mm and a mean annual temperature of 18.2°C (three year average, 2001-2003). 75% of the rainfall occurs during summer (April to September). Mean annual inorganic N deposition (from 2001-2003) was 4 g m^{-2}, 61% of which occurred in the form of NH_4^+-N (Chen and Mulder, 2007b). Data for more recent years show increasing N deposition rates to > 5 g m^{-2} yr^{-1} and confirm the relative importance of NH_4^+ (Lei Duan, *pers. comm.*). The vegetation is a coniferous-broadleaf mixed forest dominated by Masson pine (*Pinus massoniana*) with a well-developed understory of evergreen shrubs (Chen and Mulder, 2007a). Land use is a naturally regenerated, non-managed secondary forest after the original forest was cut during 1958-1962.

For the present study, a representative 4.6 ha sub-catchment was selected, consisting of a NE facing hill slope (HS) and a hydrologically connected SE - NW oriented, terraced valley bottom acting as a ground water discharge zone (GDZ) (Fig. 1b). The HS is dominated by acidic, loamy yellow mountain soils (Haplic Acrisols; WRB, 2006),

151 developed from sandstone, the predominant bedrock in the area. The soils have only a
152 thin organic layer (O horizon; 0-2 cm) (Table 1), likely reflecting high turnover rates
153 of soil organic matter (SOM) in the warm and wet climate (Raich and Schlesinger,
154 1992; Zhou et al., 2008). Soils in the GDZ have developed from colluvium (Cambisols)
155 and were terraced during the 1960s for vegetable cultivation but abandoned shortly
156 after. The soils in the GDZ have a low hydraulic conductivity (Sørbotten, 2011), lack
157 horizontal differentiation (no distinct O horizon) and have high ground water levels.
158 The vegetation in the GDZ consists of sparse shrubs and grasses while trees taller than
159 2 m are absent. Clay mineralogy on HS and in GDZ is dominated by kaolinite. A
160 recent study (Sørbotten, 2011) showed that considerable interflow occurs along HS
161 during rainfall episodes. Excess water moves laterally down slope in surface horizons
162 overlaying the argic B horizon, which has a low hydrological conductivity, thus
163 draining the O/A and AB horizons on the HS relatively quickly. Discharge of
164 interflow into GDZ results in episodically high ground water levels and periodic
165 water-logging during summer (Sørbotten, 2011). Major soil characteristics for both
166 locations are summarized in Table 1.

167 2.2 N_2O flux measurements

168 N_2O emissions were measured manually by closed chamber technique along two
169 transects in the sub-catchment. Transect (T) was established perpendicular to the
170 contour lines on the HS stretching from the hill top close to the watershed divide to

171 the hill bottom close to the GDZ. Transect (B) was established in the GDZ following
172 an elevation gradient of six hydrologically connected terraces (Fig. 1b) towards a
173 flume, which was used to measure runoff from the sub-catchment. Six plots for N_2O
174 emission measurements (n=3) and sampling of soil and pore water were established
175 along the T transect on HS (T1 to T5 and B1) and five plots along the B transect in
176 GDZ (B2 to B6; Fig. 1b) with plot B1 representing the transition between HS and
177 GDZ. Two sampling strategies were applied to explore N_2O fluxes. A first
178 measurement campaign during summer 2009 (July to September) with frequent flux
179 measurements explored N_2O emission dynamics in response to sudden increases in
180 soil moisture after rainfall episodes. A more regular sampling scheme with biweekly
181 measurements was applied throughout the dry-cool season (Nov. 2009 to Mar. 2010)
182 and during the subsequent summer (from Apr. to Aug. 2010), interrupted by more
183 intensive measurement campaigns after individual rain storms (> 20 mm). For logistic
184 reasons, only a selection of plots (T1, T3, T5, B1, B2, B4 and B6) was monitored
185 during the dry season. In total 38 triplicate flux measurements were conducted on
186 plots T1, T3, T5, B1, B2, B4 and B6 and 20 on plots T2, T4, B3 and B5.

187 For flux sampling, closed, vented, zinc-coated iron chambers (30 cm diameter and 30
188 cm in height) (Hutchinson and Mosier 1981) were carefully pushed app. 2 cm into the
189 soil. Given the loamy texture and the limited number of roots in the mostly moist
190 surface soil, this deployment method was preferred over installing permanent
191 chamber bases which might impair surface run off and interflow during rain storms.

192 The chamber deployment was quality assured by checking for deviations of initial (1
193 min after deployment) chamber N_2O concentration from ambient (~0.34 ppmv) and
194 using CO_2 accumulation over time (not shown) to check for leakage, both of which
195 were regular in most of the cases. Gas samples were taken from a sampling port on
196 top of the chambers at 1, 5, 15 and 30 minutes after deployment by a 20-ml plastic
197 syringe. Samples were transferred immediately to pre-evacuated 12 ml-vials crimp
198 sealed with butyl septa (Chromacol, UK), resulting in an overpressure to avoid
199 contamination due to pressure changes during shipment. Chamber temperature was
200 recorded by inserting a handheld digital thermometer into the sampling port at
201 beginning and end of chamber deployment. Gas samples were shipped to the
202 Norwegian University of Life Sciences and analyzed within half a year after sampling.
203 The vials kept overpressure during shipment and storage. The samples were analyzed
204 by ECD-gas chromatography (Model 7890A, Agilent, Santa Clara, CA, US). Carbon
205 dioxide (CO_2) and N_2O were separated on a 20 m wide-bore (0.53 mm diameter)
206 Poraplot Q column run at 38°C after passing a packed Heysept column used for
207 back-flushing water. Helium (He 5.0) was used as carrier gas. The ECD was run at
208 375°C with 17 ml min^{-1} Ar/CH_4 (90/10 vol%) as make-up gas. N_2O emission rates
209 (μg N m^{-2} hr^{-1}) were calculated based on the rate of change in N_2O concentration in
210 the chamber, the internal volume of the chamber, the covered soil surface area and the
211 average chamber temperature during deployment. For determining the rate of change
212 in N_2O concentration in the chamber, which is the slope of a linear or a second order

polynomial fit of the concentration data against time, the R-square of both regressions were compared. Cumulative N_2O emissions for observation periods in summer 2009 (27 days, Jul. 12 to Aug. 8) and summer 2010 (106 days, May 10 to Aug. 24) were calculated assuming a constant flux rate between sampling dates. For the calculation of cumulative N_2O emissions, only the periods with sampling frequency high enough to obtain the cumulative N_2O emission rates of the whole summer based on measurements were used.

2.3 Soil sampling and analysis

Composite soil samples were taken on Oct. 15, 2009 from the eleven plots used for N_2O flux measurements, and analyzed for pH, total organic carbon (TOC) and total nitrogen (TN). Samples at plots T1 to T5 and B1 were taken from the O- (0-2cm), A- (2-8cm), AB- (8-20cm) and B- (20-40cm) horizons. In GDZ (plots B2 to B6), where an organic horizon was absent, the homogeneous 0-20 cm and 20-40 layers were sampled. Denitrification characteristics of the soils, investigated in a laboratory study, are reported elsewhere (Zhu et al. 2013). Briefly, the instantaneous denitrification rate (expressed in nmol N_2O-N g^{-1} dw soil hr^{-1}) in soils from the different plots was estimated from the N_2O accumulation rate in acetylene-treated, anoxic soil slurries at 20^{o}C in the presence of ample NO_3^--N (2 mM). The soils' *ex situ* potential for N_2O loss (in nmol NO_3^--N g^{-1} dw soil) was estimated as the amount of NO_3^--N respired to N_2O before N_2O reductase activity was fully expressed and rapid N_2O reduction to N_2

233 occurred. Since instantaneous denitrification rates were low in the deeper horizons,
234 only data from the O and A horizons of HS and the 0-20 cm layer of GDZ are
235 presented here.

236 Soil pH (H_2O) was measured in a suspension of 10 g dry weight (dw) soil in 50 ml
237 de-ionized water with an Orion SA720 electrode pH-meter connected to an Orion
238 ROSS Ultra pH Electrode. The contents of TOC and TN in the soil were measured in
239 the fine earth fraction (< 2mm), obtained after drying at 105^{o}C and sieving, using an
240 element analyser (Vario EL III, Elementar Analysensysteme GmbH, Germany) at the
241 Research Center of Eco-environmental Science, Chinese Academy of Science
242 (RCEES, CAS). In addition, soil samples from the horizons and layers of all plots
243 were collected three times (Oct. 15, 2009, Jan. 22, 2010 and Apr. 29, 2010) to
244 measure KCl-extractable nitrate ($NO_3^-{}_{ex}$) and ammonium ($NH_4^+{}_{ex}$). After being
245 sampled, soils were stored in a freezer and extracted within one month, except the soil
246 taken on Jan. 22, 2010, which was extracted together with the samples taken on Apr.
247 29, 2010. Soil samples were extracted by shaking 10 g dw equivalents of fresh soil
248 with 50 ml of 2M KCl for 1 hr. The concentrations of NO_3^- and NH_4^+ in the filtered
249 extract were determined using Flow Injection Analysis (San^{++}, Skalar, the
250 Netherlands) at RCEES, CAS.

251 Ceramic suction cup lysimeters (P80; Staatliche Porzellanmanufaktur, Berlin) and
252 Macrorhizon soil moisture sampler (Rhizosphere Research Products, The Netherlands)

253 were installed at each plot on HS and GDZ, respectively. On the HS, lysimeters were
254 installed in triplicate in the A- (4-5 cm), the top of the AB- (10 cm), the bottom of the
255 AB- (20 cm) and in the B horizon (40 cm). In the GDZ, one Macrorhizon was
256 installed at each of three depths (30, 60 and 100 cm). Soil water from HS was
257 sampled from Nov. 11, 2009, while groundwater in the GDZ was sampled from Aug.
258 5, 2009; both soil water and groundwater were sampled at weekly intervals until
259 spring 2010 and on each N_2O flux measurement date in summer 2010. Soil water
260 from triplicate lysimeters per soil depth on HS was pooled prior to analysis.
261 Concentrations of NO_3^- and NH_4^+ in lysimeter water were measured in each sample
262 during wet-hot seasons and in pooled samples (four weeks) during the dry-cool season,
263 using ion chromatography (DX-120 for NH_4^+ and DX-500 for NO_3^-, DIONEX, USA)
264 at the Chongqing Academy of Environmental Sciences and Monitoring, China.

265 Soil bulk density (BD) of surface horizons/layers was measured from intact soil cores
266 (100cc steel cylinders) sampled in triplicate at two depths (3.5–7.2 cm and 10-13.7
267 cm), corresponding to the A and AB horizons, respectively (Sørbotten, 2011).

268 Soil temperature (ST) and volumetric moisture (VM, cm^3/cm^3) at 10 cm depth were
269 recorded every 10 minutes by TDR probes (Hydra Probe II) installed at plots T3 and
270 B1 on Oct. 11, 2009 and stored by a data logger (Campbell CR200). Data were
271 obtained until May 4, 2011, with a malfunctioning period from Dec. 25, 2010 to Feb.
272 8, 2011. Soil water filled pore space (WFPS) was calculated using bulk density (BD)

273 at depth of 10.0 - 13.7 cm, assuming a soil particle density (PD) of 2.65 g cm^{-3} (Linn
274 and Doran 1984) as:

275 $$WFPS(\%) = \frac{\mathrm{VM}}{1-(\frac{\mathrm{BD}}{\mathrm{PD}})} \times 100 \qquad \text{(Eq. 1)}$$

276 Groundwater level was monitored in PVC tubes, with a 30-cm nylon filter at the
277 lower end, and installed at each plot along the B-transect in GDZ (B1 to B6). The
278 PVC tubes were covered with a perforated lid to prevent pressure differences with the
279 atmosphere. Groundwater level was measured daily from Jul. 2009 to the beginning
280 of Aug. 2009 during a period of heavy rainstorms and on dates of N_2O measurements
281 thereafter.

282 Meteorological data (air temperature (AT), precipitation (precip) and relative
283 humidity (RH)) were obtained every 5 minutes from a weather station (WeatherHawk
284 232, USA), at the roof of the TSP Forest Bureau situated 1 km south of the catchment.
285 Vapor pressure deficit (VPD, kPa) was calculated from equation 2 (ASCE, 2005) as:

286 $$\mathrm{VPD} = \left(\frac{\mathrm{RH}}{100} - 1\right) * 0.6108 * \exp(17.27 * \mathrm{AT}/(\mathrm{AT} + 237.3) \qquad \text{(Eq. 2)}$$

287 2.4 Statistical analysis

288 Cumulative N_2O emissions for each of the eleven plots for summer 2010 (106 days)
289 were analyzed together with soil parameters in the top soil (depth-weighted for O and
290 A horizons on HS and from 0-20 cm in GDZ; Table 1) by Principal Component
291 Analysis (PCA). Bulk density, cumulative N_2O flux, $NH_4^+{}_{sw}$ and $NO_3^-{}_{sw}$ were

292 normalized using minus reciprocal, natural logarithmic, natural logarithmic and
293 sinusoidal transformation, respectively.

294 To explore the seasonal drivers of the N_2O emission flux, log-transformed average
295 N_2O emission rates on HS (average of 4 plots, T1, T3, T5 and B1, which had full N_2O
296 flux datasets including the dry season) were subjected to stepwise multiple linear
297 regression with soil temperature (ST), water filled pore space (WFPS) (average of
298 daily ST and WFPS obtained from TDR probes at both T3 and B1 from Oct. 12, 2009
299 onwards), as well as pore water $NO_3^-{}_{sw}$ and $NH_4^+{}_{sw}$ concentration in these four plots
300 as independent variables. The resulting empirical relation was used to interpolate the
301 N_2O flux on HS between measurement dates on the basis of continuously measured
302 soil temperature and WFPS and to estimate the annual N_2O emission of two complete
303 annual periods: one from May 5, 2009 to May 4, 2010 and the other one from May 5,
304 2010 to May 4, 2011.

305 Missing values for soil temperature (ST) and water filled pore space (WFPS) (from
306 May 1 to Oct. 11, 2009 and from Dec. 25, 2010 to Feb. 8, 2011) were estimated on a
307 daily basis, using a statistical model based on multiple linear regression, using
308 available meteorological data (average air temperature, rainfall and average VPD).
309 General linear model (GLM) with the mixed-effects (sampling dates and location)
310 was used for the comparison of different plots, the two landscape elements and
311 different seasons.

All statistical analyses were conducted with Minitab 16.1.1 (Minitab Inc.).

3. Results

3.1 Weather, soil moisture and soil temperature

Rainfall distribution during the wet season (Apr. to Oct.) differed between the two years (Fig. 2). Summer 2009 (1054 mm) was wetter than summer 2010 (850 mm) and precipitation occurred mostly as intensive rainstorms (up to 385 mm during 41 hours between 3rd and 5th of Aug. 2009). In contrast, precipitation was more evenly distributed in summer 2010. Only 117 mm rain fell in the dry-cool season from November 2009 to March 2010. Soil water filled pore space (WFPS) at 10 cm depth on the mid slope (T3, mean WFPS 55.8%) was significantly smaller than at the foot slope of HS at the transition to GDZ (B1, mean WFPS 70.0%) (Fig. 3a), most likely reflecting convergence of interflow from HS at B1. In winter, water filled pore space (WFPS) was relatively stable with values around 56.7% for T3 and 68.5% for B1. In contrast, large variations in water filled pore space (WFPS) were observed in spring and summer, driven by precipitation, and subsequent drainage and evapotranspiration. In plot T3 (HS), but not in plot B1 (transition to GDZ), water filled pore space (WFPS) decreased significantly in late summer 2010 (July through September), indicating drier conditions on the upper part of HS as described earlier for this site (Mulder et al., 2005). Soil temperature at 10 cm depth varied seasonally between 10^{o}C and 25^{o}C with no significant difference between T3 and B1, although the drier T3 plot tended to have somewhat higher soil temperatures during the wet season (Fig. 3b).

334 The groundwater level in GDZ varied between +15 cm (above surface) and < –100
335 cm (below surface), with highest values at B5 and lowest at B1 (Fig. 4). The heavy
336 rainstorm between Aug. 3rd and 5th, 2009 resulted in a rapid increase of the
337 groundwater level. The groundwater level reached its lowest values from late summer
338 onwards, but increased in early spring, due to increased precipitation in Mar. and Apr.,
339 2010. In general, the groundwater level was deepest at B1 and increased to
340 near-surface in the order B1<B2=B3=B4<B5<B6 and was most stable close to the
341 outlet (plots B5 and B6). The groundwater level was only occasionally detectable
342 (>-100 cm depth) at plots B1, B2 and B3 (Fig. 4).

343 3.2 N_2O fluxes

344 Emission fluxes of N_2O showed a pronounced seasonal pattern with highest values
345 during summer (wet-hot season) and significantly lower emission rates during winter
346 (dry-cool season) (p=0.000, Fig. 5). During summer, N_2O emission rates varied 1-2
347 orders of magnitude, with highest values immediately following precipitation events
348 (compare Figs. 2 and 5) when water filled pore space (WFPS) was high (Fig. 3a). In
349 summer 2010, with its more even distribution of rainfall, peak N_2O emissions were
350 smaller (up to 450 μg m^{-2} hr^{-1}) than in summer 2009 (up to 1730 μg N m^{-2} hr^{-1}) (Fig.
351 5). The analysis with a general linear model (GLM) indicated that N_2O emission rates
352 were significantly higher on HS than in GDZ (p=0.011). The daily average N_2O
353 emission on HS was higher in summer 2009 (6.4 mg N m^{-2} d^{-1}) than in summer 2010

354 (3.2 mg N m^{-2} d^{-1}; Fig. 6). Furthermore, the average N_2O emission was smaller in
355 GDZ than on HS, emitting in average 3.2 mg N_2O-N m^{-2} d^{-1} and 1.8 mg N_2O-N m^{-2}
356 d^{-1} in 2009 and 2010, respectively. The spatial variability within the plots was high
357 particularly on HS (Fig. 6) and no significant differences in N_2O emissions were
358 found between plots within the same landscape element. The spatial pattern of the
359 cumulative N_2O emissions for the plots within one transect was not consistent for the
360 two summer periods (Fig. 6).

361 3.3 Spatial variability in soil factors controlling N_2O emissions

362 Surface soil had a greater bulk density in GDZ than on HS (Table 1) even though
363 there were exceptions (plots B4 and B5). The pH of the surface soil was significantly
364 higher in GDZ than on HS (Table 1). For TOC, TN and C/N the opposite was the case,
365 reflecting the lack of an organic surface layer in GDZ. Values for the concentration of
366 NO_3^- in soil extracts ($NO_3^-_{ex}$) and the concentration of NO_3^- in soil water ($NO_3^-_{sw}$)
367 were significantly higher on HS than in GDZ. In the O-horizon, TOC and TN were
368 higher at T2 and T4 than at other plots on HS. In the GDZ, Plot B6 was highest with
369 respect to these variables. The $NO_3^-_{sw}$ was high in winter and early spring and
370 decreased sharply at the start of the growing season in early April, probably due to
371 biological uptake of N and dilution by ample rainfall at the end of March 2010 (Fig.
372 7). During winter, $NO_3^-_{sw}$ showed consistent differences among plots on HS with
373 highest values at plot T1 and lowest at plot T2, whereas concentrations were lower

374 and more uniform throughout summer, fluctuating with precipitation events. There
375 were consistent differences in $NO_3^-{}_{sw}$ in GDZ, with concentration levels decreasing in
376 the order B2 = B4 > B3 > B5 ≥ B6. At B3, B5 and B6, $NO_3^-{}_{sw}$ concentrations were
377 below 5 mg N L^{-1} during most of the year with the greatest values at the end of the dry
378 season (Feb. and Mar., 2010). The concentration of NH_4^+ in soil water ($NH_4^+{}_{sw}$) was
379 small, with values amounting to less than 10% of total inorganic N in solution, except
380 for plots B2 and B6, and there was no seasonal pattern in any of the plots (data not
381 shown). No correlation was found between $NH_4^+{}_{sw}$ and $NO_3^-{}_{sw}$ in soil water.

382 We used PCA to assess the relationship between soil parameters and the cumulative
383 N_2O flux in summer 2010 (Fig. 6) at each plot (Fig. 8). The PCA divided the plots
384 into two groups (T1 to T5 and B1 as one group (HS); the others as the second group
385 (GDZ)). The first two components of PCA explained 63.9% of the total variation,
386 with most of the physicochemical parameters (pH, bulk density, TOC, TN, $NO_3^-{}_{ex}$,
387 $NO_3^-{}_{sw}$ and $NH_4^+{}_{ex}$) and the *ex situ* potential for N_2O loss contributing to the first
388 component (50.3%). The second component (13.6%) included $NH_4^+{}_{sw}$. The
389 instantaneous denitrification rate contributed to both components, but had relatively
390 small effect on the N_2O flux compared to other parameters. Total organic carbon
391 (TOC) and most of the variables associated with the availability of N (TN, $NO_3^-{}_{ex}$,
392 $NO_3^-{}_{sw}$ and $NH_4^+{}_{ex}$) were positively correlated with soil N_2O flux, whereas soil pH and
393 bulk density (BD) were negatively correlated with N_2O flux. Also, the instantaneous
394 denitrification rate and the *ex situ* potential for N_2O loss were positively correlated

with N_2O flux, whereas $NH_4^+{}_{sw}$ concentration in soil water did not correlate with N_2O flux.

3.4 Temporal variability of seasonal drivers for N_2O emission

In summer, peak N_2O emission was associated with rainfall resulting in high water filled pore space (WFPS) values. Emission of N_2O on HS was highest at water filled pore space (WFPS) values between 63% and 72% (averages at 10 cm soil depth for T3 and B1, respectively) and appeared somewhat lower at values larger than 75% (Figs. 3a and 5). Figure 5 illustrates the large inter-annual variability of N_2O flux between a wet year with intensive rainfall episodes (2009) and a relatively dry year (2010) with only one episode with precipitation > 50 mm day^{-1} (82 mm in 9 hrs on July 5, 2010). The N_2O flux on HS was weakly, but negatively correlated with $NO_3^-{}_{sw}$ ($p=0.064$) whereas no correlation was found with $NH_4^+{}_{sw}$ ($p=0.659$). At individual sites in GDZ, the N_2O flux was weakly, but negatively correlated with the groundwater level, i.e. higher N_2O flux occurred when the groundwater level was low. Low soil temperature (ST) together with low water filled pore space (WFPS) seemed to be the main constraints for N_2O emission activity in winter (Figs. 3 and 5). Stepwise multiple linear regression indicated that soil temperature (ST) and water filled pore space (WFPS) were the only significant variables explaining temporal variability of N_2O emissions (Eq. 3) on HS; $NO_3^-{}_{sw}$ and $NH_4^+{}_{sw}$ concentrations did not add significantly and were excluded by the regression. The residuals of the simulated

415 values were normally distributed (not shown), suggesting unbiased fitting of the
416 equation (standard errors of the coefficients in parenthesis):

417 $$\ln(\mathrm{N2O_{HS}}) = -4.80\ (\pm 1.24) + 0.088\ (\pm 0.018)\ \mathrm{WFPS} + 0.178\ (\pm 0.024)\ \mathrm{ST}$$

418 (Eq. 3)

419 Adjusted coefficient of determination (R-Sq(adj)) = 68.9%

420 Since no data for soil temperature (ST) and water filled pore space (WFPS) was
421 available before Oct. 11, 2009 and from Dec. 25, 2010 to Feb. 8, 2011, we used
422 multiple linear regression to derive an equation that links soil temperature (ST) and
423 water filled pore space (WFPS) to meteorological data. The resulting regression
424 models, presented in equations 4 and 5 were then used to estimate the missing values
425 (standard errors of the coefficients in parenthesis):

426 $$\mathrm{ST} = 7.84\ (\pm 0.41) + 0.579\ (\pm 0.029)\ \mathrm{AT} + 1.20\ (\pm 0.187)\ \mathrm{VPD} \qquad \text{(Eq. 4)}$$

427 Adjusted coefficient of determination (R-Sq(adj)) = 67.4%

428 $$\mathrm{WFPS} = 63.2\ (\pm 0.27) + 0.209\ (\pm 0.014)\ \mathrm{precip_5} + 1.84\ (\pm 0.17)\ \mathrm{VPD_5} \qquad \text{(Eq. 5)}$$

429 Adjusted coefficient of determination (R-Sq(adj)) = 58.8%

430 where $precip_5$ (mm) is the day-weighted 5-day average precipitation prior to the date
431 for which the computation was done (calculated as $1.0*\mathrm{precip_{day(0)}} + 0.8*\mathrm{precip_{day(-1)}} +$
432 $0.6*\mathrm{precip_{day(-2)}} + 0.4*\mathrm{precip_{day(-3)}} + 0.2*\mathrm{precip_{day(-4)}}$) and VPD_5 (kPa) the
433 day-weighted 5-day average vapor pressure deficit calculated analogously. The

434 selected weights fitted the observations best. The residuals of the model simulations
435 were normally distributed (not shown). Equation 3 was used to estimate N_2O
436 emissions using measured and simulated values for soil temperature (ST; Eq. 4) and
437 water filled pore space (WFPS; Eq. 5). Measured and simulated values are shown in
438 figure 9.

439 3.5 Annual N_2O flux

440 Annual N_2O emissions on the HS were calculated at a daily time step from equation 3
441 for two 1-year periods (May 5 2009 – May 4 2010 and May 5 2010 to May 4, 2011)
442 (Fig. 9). The first annual period included a relatively wet summer, whereas the second
443 period had a relatively dry summer. Annual N_2O fluxes for HS were 0.54 and 0.43 g
444 N m^{-2} for the two years, respectively, about 24% higher in the first year than in the
445 second. Higher annual N_2O emission in the first year may be attributed to the
446 contribution of the frequent rain episodes in the wet summer of 2009. The N_2O
447 emission occurring during the first 5 days after the largest rainfall episode (Aug. 4 to
448 5, 2009) contributed 15.8% to the annual N_2O emission. Emissions during the
449 dry-cool season in the first year (November 2009 to March 2010) contributed 12.0%
450 to the annual flux of N_2O. Also the emissions during the dry-cool season in the second
451 year (November 2010 to March 2011), solely based on model estimates, was found to
452 be low, contributing 16.9% to the annual flux of N_2O.

453

4. Discussion

N_2O emission rates recorded after the heavy rainstorm in 2009 (up to 1730 µg N_2O-N m^{-2} hr^{-1}; Fig. 5) are the highest found for forest ecosystems so far and exceed rates reported for (sub)tropical forests which typically vary between 11 to 600 µg N_2O-N m^{-2} hr^{-1} (Liu et al., 2011a; Zhang et al., 2008; Silver et al., 2005; Ishizuka et al., 2005; Koehler et al., 2009; Rowlings et al., 2012; Kiese and Butterbach-Bahl, 2002).

Temporal variability (Fig. 5) exceeded spatial variability in both landscape elements (HS and GDZ). However, small-scale (within-plot) variability of the cumulative N_2O flux over the active season was high as seen from the high standard errors in figure 6 (particularly for HS). Probably this small scale variability was blurring existing trends in flux strength between plots along the HS. Large small-scale spatial variability of N_2O emissions is often reported for forest soils (Robertson and Klemedtsson, 1996; Bowden et al., 1992; Werner et al., 2007b) and is commonly attributed to small-scale variation in mineral N availability, litter quality and soil moisture. We arranged the plots along transects perpendicular to the contour lines in the two landscape units because gradients in water filled pore space on HS and in groundwater level in GDZ might affect N_2O emissions by controlling aeration, substrate level and ultimately microbial activity (Garten et al., 1994). However, we did not find any consistent relationship between cumulative N_2O emission and plot position in either of the two landscape elements. Concentrations of $NO_3^-{}_{sw}$ on HS were similar at all plots during

474 the wet-hot season (Fig. 7a) and did not correlate with N_2O emissions. The
475 availability of NO_3^- was higher than in other studies (e.g., Koehler et al., 2009; Zhang
476 et al., 2008) and appeared to be non-limiting for N_2O production on the HS, probably
477 explaining the lack of a directional gradient in cumulative N_2O emissions as reported
478 by others (Nishina et al., 2009; Fang et al., 2009). Surprisingly, the clear difference in
479 water filled pore space between the mid slope position T3 and the foot slope position
480 B1 (Fig. 3a) in spring and early summer did not result in significantly different
481 cumulative N_2O emissions (Fig. 6). This was probably due to the fact that soil
482 moisture was measured at 10 cm depth (in the upper AB-horizon), rather than in the
483 zone of maximum denitrification activity, located in the uppermost soil layers (O and
484 A horizons; Zhu et al., 2013). Soil moisture data records for 5 cm depth were
485 incomplete due to sensor problems, but comparing existing data and bulk densities at
486 5 cm depth suggests that water filled pore space was more similar in the uppermost
487 soil layer (data not shown). The pronounced decrease in water filled pore space at T3
488 (but not B1), later in summer, markedly reduced N_2O emissions as compared with B1
489 (insert Fig. 5).

490 In GDZ, decreasing NO_3^- concentrations along the hydrological flow path (Fig. 7b)
491 suggested strong N retention. Both NO_3^- and the dissolved N_2O (data not shown)
492 concentrations in the groundwater were found to be very low at the outlet of GDZ (B5
493 and B6), suggesting more complete N_2O reduction along the flow path as NO_3^-
494 became depleted. There was a weak trend of decreasing cumulative N_2O emissions

495 with increasing average groundwater level along the hydrological flow path in the
496 GDZ (with the exception of B3) during summer 2009, when the groundwater level
497 was very dynamic (Fig. 6a). No such pattern was seen in the hydrologically more
498 stable summer of 2010 (Fig. 6b). In general, groundwater level fluctuations are likely
499 to interact with NO_3^- in controlling N_2O emissions, as the rise of groundwater level
500 can transport NO_3^- into C-richer upper soil layers and create anoxia favorable for
501 denitrification. At the same time, the residence time of N_2O in the soil profile
502 increases, due to decreasing diffusion, thus increasing the chance of N_2O being
503 reduced to N_2. Conversely, a drop in groundwater level may relieve gaseous diffusion
504 constraints leading to release of N_2O from the soil. In summer 2010 (Fig. 5), for
505 instance, N_2O emission rates were lowest at B6 until groundwater level dropped about
506 10 cm in the middle of July (Fig. 4), resulting in a single N_2O emission peak while
507 returning to low levels quickly thereafter. Similar N_2O dynamics have been observed
508 in rice paddies (e.g. Qin et al., 2010).

509 We found clear differences in N_2O source strength and environmental controls when
510 comparing HS and GDZ; average cumulative N_2O emission in GDZ was roughly half
511 of this at HS in both summers (Figs. 5 and 6), which was surprising, as we expected
512 GDZ to behave as a riparian zone with elevated denitrification activity. Riparian
513 zones are commonly considered as "hot spots" for N_2O emissions, because they
514 receive dissolved N (DON, NO_3^-) from surrounding slopes while providing optimal
515 conditions for denitrification (DOC, anoxia) (Groffman et al., 2000; Hefting et al.,

516 2003). However, unlike common riparian zones which typically develop soils rich in
517 organic matter, the GDZ studied here is formed by formerly cultivated terraces on
518 colluvial deposits. Soils are dense and have low hydrological conductivities, resulting
519 in low productivity and low TOC contents (Table 1). Laboratory incubations revealed
520 that the GDZ soils had instantaneous denitrification rates similar to HS soils, despite
521 their markedly lower TOC contents (Zhu et al. 2013). This indicated a similar N
522 removal potential in GDZ as compared with HS. However in their study, Zhu et al.
523 (2013) also found that denitrifying communities on HS and in GDZ differed
524 functionally with respect to their product stoichiometry, with the GDZ communities
525 being more efficient in reducing NO_3^- all the way to N_2. Thus, the lower N_2O/N_2 ratio,
526 and consequently the reduced N_2O emission rate, in GDZ may be attributed to a
527 number of site-specific factors, directly or indirectly affecting denitrifier functioning
528 and stoichiometry: 1) pore water at GDZ had lower NO_3^- concentrations (Figs. 7b and
529 8) which may decrease the N_2O/N_2 ratio by forcing denitrifiers to utilize N_2O as an
530 additional electron acceptor; 2) diffusion of N_2O in soil is slow in dense GDZ soils,
531 resulting in higher dissolved N_2O concentrations in pore water (data not shown)
532 which supports denitrifier communities to express N_2O reductase and 3) soil pH at
533 GDZ was 0.5-0.6 units higher than at HS, which directly (Bergaust et al., 2010) or
534 indirectly (Liu et al., 2010a; Simek and Cooper, 2002; Dörsch et al., 2012) lowers
535 N_2O/N_2 ratios.

536 Even though this study was not designed to discriminate sources of N_2O emission,
537 several observations indicate that N_2O emission rates during the active periods were
538 more sensitive to denitrification controls than nitrification controls: 1) on the HS, high
539 N_2O emission occurred when soil water filled pore space was high; 2) in the GDZ,
540 dissolved N_2O decreased with NO_3^- concentration in groundwater; 3) the difference in
541 magnitude in N_2O flux on HS and in GDZ was congruent to differences in
542 denitrification stoichiometry observed in soils from the two landscape elements in
543 laboratory incubations (Zhu et al., 2013); 4) N_2O concentrations measured in soil air
544 were negatively correlated with pO_2 (R^2=0.40, p=0.000, data not shown). Low
545 nitrification rates have been reported for acidic forest soils in SW China (Cai and
546 Zhao, 2009). However, given the prevalence of NH_4^+ in deposited N and its rapid
547 disappearance in the soil solution, NH_4^+ oxidizing processes could be a potentially
548 important source for N_2O emission. We conducted an *in situ* $^{15}NO_3^-$ labeling
549 experiment in summer 2010 at two positions along the HS reported elsewhere (Zhu et
550 al., *submitted*) and found that 70-100% of the emitted N_2O derived from the labeled
551 soil NO_3^- pool. It seemed that even though the fate of the deposited NH_4^+ remains
552 unclear in this catchment, nitrification is not the main source for the high N_2O
553 emission observed.

554 We found large temporal variability in N_2O fluxes. Multiple linear regression
555 identified soil temperature and water filled pore space as the main drivers, explaining
556 68.9% of the temporal variability of N_2O emission fluxes on HS. Such a high

557 coefficient of determination with only two variables is remarkable as most studies
558 conducted in forest ecosystems report much lower degree of explanation by ancillary
559 variables (Morishita et al., 2011; Gu et al., 2011). As shown in figure 9, the resulting
560 regression model captured reasonably well both the seasonal distribution of emission
561 fluxes and the transient emission peaks after rainfall events on HS except for the first
562 measurement point. Peak N_2O emissions (Fig. 5) were triggered by spikes in water
563 filled pore space (Fig. 3a) occurring after big rain episodes, resulting in a highly
564 skewed distribution of N_2O fluxes as found in many other studies (Khalil et al., 2007;
565 Venterea et al., 2009). Low soil temperature, together with relatively low water filled
566 pore space throughout winter resulted in low N_2O fluxes. This implies that N_2O
567 emission fluxes can be estimated fairly well from discontinuous flux measurements
568 when continuous data on soil temperature and water filled pore space are available.
569 However, it is important to sample fluxes closely around major rain fall events in
570 summer as they contribute disproportionally to overall emissions. Too long interval
571 between samplings may result in over- or under-estimation of the cumulative flux
572 (Parkin, 2008).

573 Annual N_2O emissions for the TSP catchment were estimated for the HS only, since
574 96.4% of the area consists of hill slopes, rendering GDZ emissions a minor
575 component of the overall N_2O budget. Annual fluxes showed considerable variation
576 between the wet year (May. 2009 to Apr. 2010) with several intensive rain episodes
577 (0.54 g N_2O-N m^{-2} yr^{-1}) and the dryer year (May. 2010 to Apr. 2011) with more

578 evenly distributed precipitation (0.43 g N_2O-N m^{-2} yr^{-1}). The average annual N_2O
579 emission flux in TSP (0.48 g N m^{-2} yr^{-1}) is at the high end of annual N_2O emission
580 fluxes (0.005-0.47 g N m^{-2} yr^{-1}) reported for unfertilized forestland in China (Cai,
581 2012). The fluxes are even comparable to the high end of reported N_2O fluxes in
582 tropical rainforests where temperatures are high throughout the year (Dalal and Allen,
583 2008) and to a tropical lowland forest in Panama which was experimentally
584 N-enriched for 9-10 years (Koehler et al., 2009). Expressed as a fraction of the annual
585 atmogenic N-deposition, N_2O-N emission amounted to between 8 and 10% of the
586 incoming inorganic N. This "emission factor" was much higher than the Tier 1 IPCC
587 default factor (1%) used for accounting both direct N_2O emissions arising from
588 mineral N fertilizer application to managed soils and indirect N_2O emissions arising
589 from the re-deposited N to uncultivated soils (IPCC, 2006). The emission factor
590 derived from our study is at the high end of the reported N_2O emission factors for
591 deciduous forests and coniferous forests, which were on average 6.5% and 2.4%,
592 respectively (van der Gon and Bleeker 2005). This pinpoints the prominent role of
593 nitrogen saturated, subtropical forests on acid soils as a secondary source of
594 anthropogenic N_2O which should be taken into account for regional N_2O budgets.

595 **Acknowledgement**

596 This study was supported by the Norwegian research council (Nordklima program
597 193725/S30: "N_2O emissions from N saturated subtropical forest in South China")
598 and the Chinese Academy of Sciences (No. KZCX2-YW-GJ01 and GJHZ1205). We
599 are grateful for technical support by Zhang Guanli at the Chongqing Academy of
600 Environmental Sciences, Prof. Zhang Xiaoshan at the Research Center for
601 Eco-environmental Sciences, Chinese Academy of Sciences and T. Fredriksen at the
602 Norwegian University of Life Sciences. We also thank Prof. Duan Lei at the Tsinghua
603 University for providing N deposition data and L.E. Sørbotten and J. Stolte (both
604 Bioforsk, Norway) for data on soil hydrology and assistance in the field.

References:

Aber, J. D., Goodale, C. L., Ollinger, S. V., Smith, M. L., Magill, A. H., Martin, M. E., Hallett, R. A., and Stoddard, J. L.: Is nitrogen deposition altering the nitrogen status of northeastern forests?, Bioscience, 53, 375-389, 2003.

ASCE, S. o. R. E. T. C. o.: The ASCE standardized reference evapotranspiration equation, environmental and water resources, Institute of the American Society of Civil Engineers, 2005.

Banerjee, S., and Siciliano, S. D.: Factors driving potential ammonia oxidation in Canadian arctic ecosystems: does spatial scale matter?, Appl. Environ. Microbiol., 78, 346-353, 2012.

Bergaust, L., Mao, Y. J., Bakken, L. R., and Frostegard, A.: Denitrification response patterns during the transition to anoxic respiration and posttranscriptional effects of suboptimal pH on nitrogen oxide reductase in *Paracoccus denitrificans*, Appl. Environ. Microbiol., 76, 6387-6396, 2010.

Bowden, W. B., Mcdowell, W. H., Asbury, C. E., and Finley, A. M.: Riparian nitrogen dynamics in 2-geomorphologically distinct tropical rain-forest watersheds - nitrous-oxide fluxes, Biogeochemistry, 18, 77-99, 1992.

Cai, Z. C., and Zhao, W.: Effects of land use types on nitrification in humid subtropical soils of China, Acta Pedologica Sinica (in Chinese), 46, 7, 2009.

Cai, Z. C.: Greenhouse gas budget for terrestrial ecosystems in China, Sci. China-Earth Sci., 55, 173-182, 2012.

Chen, X. Y., and Mulder, J.: Indicators for nitrogen status and leaching in subtropical forest ecosystems, South China, Biogeochemistry, 82, 165-180, 2007a.

Chen, X. Y., and Mulder, J.: Atmospheric deposition of nitrogen at five subtropical forested sites in South China, Sci. Total Environ., 378, 317-330, 2007b.

D'Amelio, M. T. S., Gatti, L. V., Miller, J. B., and Tans, P.: Regional N_2O fluxes in Amazonia derived from aircraft vertical profiles, Atmos Chem Phys, 9, 8785-8797, 2009.

Dörsch, P., Braker, G., and Bakken, L. R.: Community specific pH response of denitrification: experiments with cells extracted from organic soils, FEMS Microbiology Ecology, 79, 530–541, 2012.

Dalal, R. C., and Allen, D. E.: Greenhouse gas fluxes from natural ecosystems, Aust J Bot, 56, 369-407, 2008.

De Boer W., and Kowalchuk G.A.. 2001. Nitrification in acid soils: micro-organisms and mechanisms. Soil Biology & Biochemistry 33: 853-866.

Fang, Y. T., Gundersen, P., Zhang, W., Zhou, G. Y., Christiansen, J. R., Mo, J. M., Dong, S. F., and Zhang, T.: Soil-atmosphere exchange of N_2O, CO_2 and CH_4 along a slope of an evergreen broad-leaved forest in southern China, Plant and Soil, 319, 37-48, 2009.

644 Flessa, H., Dörsch, P., and Beese, F.: Seasonal-variation of N_2O and CH_4 fluxes in
645 Difeerently managed arable soils in southern Germany, Journal of Geophysical
646 Research-Atmospheres, 100, 23115-23124, 1995.
647 Garten, C. T., Huston, M. A., and Thoms, C. A.: Topgraphic variation of soil-nitrogen
648 dynamics at Walker Branch watershed, Tennessee, Forest Sci, 40, 497-512, 1994.
649 Groffman, P. M., Gold, A. J., and Addy, K.: Nitrous oxide production in riparian
650 zones and its importance to national emission inventories, Chemosphere - Global
651 Change Science, 2, 9, 2000.
652 Gu, J. X., Nicoullaud, B., Rochette, P., Pennock, D. J., Henault, C., Cellier, P., and
653 Richard, G.: Effect of topography on nitrous oxide emissions from winter wheat
654 fields in Central France, Environmental Pollution, 159, 3149-3155, 2011.
655 Hefting, M. M., Bobbink, R., and de Caluwe, H.: Nitrous oxide emission and
656 denitrification in chronically nitrate-loaded riparian buffer zones, Journal of
657 Environmental Quality, 32, 1194-1203, 2003.
658 Hirsch, A. I., Michalak, A. M., Bruhwiler, L. M., Peters, W., Dlugokencky, E. J., and
659 Tans, P. P.: Inverse modeling estimates of the global nitrous oxide surface flux
660 from 1998-2001, Global Biogeochemical Cycles, 20, 2006.
661 Hutchinson, G. L., and Mosier, A. R.: Improved soil cover method for field
662 measurement of nitrous oxide fluxes, Soil Science Society of America Journal, 45,
663 311-316, 1981.
664 IPCC (2007) Summary for policy makers. In: *Climate Change 2007: The physical*
665 *Science Basis. Contribution of Working Group I to the Fourth Assessment Report*
666 *of the Intergovernmental Panel on Climate Change.* (eds Solomon S, Qin D,
667 Manning M, Chen Z, Marquis M, Averyt KB, Tignor M, Miller HL), Cambridge,
668 UK and New York, USA. 2007.
669 IPCC (2006) Agriculture, Forestry and Other Land Use. In: *Guidelines for National*
670 *Greenhouse Gas Inventories.* (eds Eggleston H.S., Buendia L., Miwa K., Ngara T.
671 and Tanabe K.), IGES, Japan. 2006.
672 Ishizuka, S., Iswandi, A., Nakajima, Y., Yonemura, L., Sudo, S., Tsuruta, H., and
673 Muriyarso, D.: Spatial patterns of greenhouse gas emission in a tropical rainforest
674 in Indonesia, Nutrient Cycling in Agroecosystems, 71, 55-62, 2005.
675 Khalil, M. I., Van Cleemput, O., Rosenani, A. B., and Schmidhalter, U.: Daytime,
676 temporal, and seasonal variations of N_2O emissions in an upland cropping system
677 of the humid tropics, Communications in Soil Science and Plant Analysis, 38,
678 189-204, 2007.
679 Kiese, R., and Butterbach-Bahl, K.: N_2O and CO_2 emissions from three different
680 tropical forest sites in the wet tropics of Queensland, Australia, Soil Biology &
681 Biochemistry, 34, 975-987, 2002.
682 Koehler, B., Corre, M. D., Veldkamp, E., Wullaert, H., and Wright, S. J.: Immediate
683 and long-term nitrogen oxide emissions from tropical forest soils exposed to
684 elevated nitrogen input, Global Change Biology, 15, 2049-2066, 2009.

685 Kort, E. A., Patra, P. K., Ishijima, K., Daube, B. C., Jimenez, R., Elkins, J., Hurst, D.,
686 Moore, F. L., Sweeney, C., and Wofsy, S. C.: Tropospheric distribution and
687 variability of N_2O: Evidence for strong tropical emissions, Geophys Res Lett, 38,
688 2011.
689 Lark, R. M., Milne, A. E., Addiscott, T. M., Goulding, K. W. T., Webster, C. P., and
690 O'Flaherty, S.: Scale- and location-dependent correlation of nitrous oxide
691 emissions with soil properties: an analysis using wavelets, Eur. J. Soil Sci., 55,
692 611-627, 2004.
693 Larssen, T., Duan, L., and Muder, J.: Deposition and leaching of sulfur, nitrogen and
694 calcium in four forested catchments in China: implications for acidification,
695 Environmental Science & Technology, 45, 1192-1198, 2011.
696 Linn D.M., and Doran J.W.. 1984. Effect of water-filled pore-space oon carbon
697 dioxide and nitrous oxide productioon in tilled and nontilled soils. Soil Science
698 Society of America Journal 48: 1267-1272.
699 Lin, S., Iqbal, J., Hu, R. G., and Feng, M. L.: N_2O emissions from different land uses
700 in mid-subtropical China, Agric. Ecosyst. Environ., 136, 40-48, 2010.
701 Lin, S., Iqbal, J., Hu, R. G., Ruan, L. L., Wu, J. S., Zhao, J. S., and Wang, P. J.:
702 Differences in nitrous oxide fluxes from red soil under different land uses in
703 mid-subtropical China, Agric. Ecosyst. Environ., 146, 168-178, 2012.
704 Liu, B. B., Morkved, P. T., Frostegard, A., and Bakken, L. R.: Denitrification gene
705 pools, transcription and kinetics of NO, N_2O and N_2 production as affected by
706 soil pH, FEMS Microbiol. Ecol., 72, 407-417, 2010a.
707 Liu, B. B., Morkved, P. T., Frostegard, A., and Bakken, L. R.: Denitrification gene
708 pools, transcription and kinetics of NO, N_2O and N_2 production as affected by
709 soil pH, FEMS Microbiol. Ecol., 72, 407-417, 2010b.
710 Liu, J., Jiang, P. K., Li, Y. F., Zhou, G. M., Wu, J. S., and Yang, F.: Responses of
711 N_2O Flux from Forest Soils to Land Use Change in Subtropical China, Bot. Rev.,
712 77, 320-325, 2011a.
713 Liu, X. J., Duan, L., Mo, J. M., Du, E. Z., Shen, J. L., Lu, X. K., Zhang, Y., Zhou, X.
714 B., He, C. N., and Zhang, F. S.: Nitrogen deposition and its ecological impact in
715 China: An overview, Environmental Pollution, 159, 2251-2264, 2011b.
716 Melillo, J. M., Steudler, P. A., Feigl, B. J., Neill, C., Garcia, D., Piccolo, M. C., Cerri,
717 C. C., and Tian, H.: Nitrous oxide emissions from forests and pastures of various
718 ages in the Brazilian Amazon, Journal of Geophysical Research-Atmospheres,
719 106, 34179-34188, 2001.
720 Morishita, T., Aizawa, S., Yoshinaga, S., and Kaneko, S.: Seasonal change in N_2O
721 flux from forest soils in a forest catchment in Japan, J. For. Res., 16, 386-393,
722 2011.
723 Mørkved, P. T., Dörsch, P., and Bakken, L. R.: The N_2O product ratio of nitrification
724 and its dependence on long-term changes in soil pH, Soil Biology &
725 Biochemistry, 39, 2048-2057, 2007.

726 Mulder, J., Chen, X. Y., Zhao, D. W., and Xiang, R. J.: Elevated nitrogen deposition
727 in subtropical Chinese forest ecosystems, dominated by Masson pine: Nitrogen
728 fluxes and budgets at the plot and catchment scale, The 3rd international N
729 conference, Nanjing, China, Oct.12-16, 2004, 2005.
730 Nishina, K., Takenaka, C., and Ishizuka, S.: Spatiotemporal variation in N_2O flux
731 within a slope in a Japanese cedar (Cryptomeria japonica) forest,
732 Biogeochemistry, 96, 163-175, 2009.
733 Osaka, K., Ohte, N., Koba, K., Katsuyama, M., and Nakajima, T.: Hydrologic
734 controls on nitrous oxide production and consumption in a forested headwater
735 catchment in central Japan, J. Geophys. Res.-Biogeosci., 111, 11, G01013, 2006.
736 Parkin, T. B.: Effect of sampling frequency on estimates of cumulative nitrous oxide
737 emissions, Journal of Environmental Quality, 37, 1390-1395, 2008.
738 Parton, W. J., Mosier, A. R., Ojima, D. S., Valentine, D. W., Schimel, D. S., Weier,
739 K., and Kulmala, A. E.: Generalized model for N_2 and N_2O production from
740 nitrification and denitrification, Global Biogeochemical Cycles, 10, 401-412,
741 1996.
742 Philippot, L., Cuhel, J., Saby, N. P. A., Cheneby, D., Chronakova, A., Bru, D.,
743 Arrouays, D., Martin-Laurent, F., and Simek, M.: Mapping field-scale spatial
744 patterns of size and activity of the denitrifier community, Environ Microbiol, 11,
745 1518-1526, 2009.
746 Qin, Y. M., Liu, S. W., Guo, Y. Q., Liu, Q. H., and Zou, J. W.: Methane and nitrous
747 oxide emissions from organic and conventional rice cropping systems in
748 Southeast China, Biology and Fertility of Soils, 46, 825-834, 2010.
749 Raich, J. W., and Schlesinger, W. H.: The global carbon dioxide flux in soil
750 respiration and its relationship to vegetation and climate, Tellus B, 44, 81-99,
751 1992.
752 Robertson, K., and Klemedtsson, L.: Assessment of denitrification in organogenic
753 forest soil by regulating factors, Plant Soil, 178, 49-57, 1996.
754 Rowlings, D. W., Grace, P. R., Kiese, R., and Weier, K. L.: Environmental factors
755 controlling temporal and spatial variability in the soil-atmosphere exchange of
756 CO_2, CH_4 and N_2O from an Australian subtropical rainforest, Global Change
757 Biology, 18, 726-738, 2012.
758 Sørbotten, L.: Hill slope unsaturated flowpaths and soil moisture variability in a
759 forested catchment in southwest China, Master, Department of Plant and
760 environmental sciences, Norwegian Univerisity of Life Sciences, Aas, 64 pp.,
761 2011.
762 Silver, W. L., Thompson, A. W., McGroddy, M. E., Varner, R. K., Dias, J. D., Silva,
763 H., Crill, P. M., and Keller, M.: Fine root dynamics and trace gas fluxes in two
764 lowland tropical forest soils, Global Change Biology, 11, 290-306, 2005.
765 Simek, M., and Cooper, J. E.: The influence of soil pH on denitrification: progress
766 towards the understanding of this interaction over the last 50 years, Eur. J. Soil
767 Sci., 53, 345-354, 2002.

768 Smith, K. A., Ball, T., Conen, F., Dobbie, K. E., Massheder, J., and Rey, A.:
769 Exchange of greenhouse gases between soil and atmosphere: interactions of soil
770 physical factors and biological processes, Eur. J. Soil Sci., 54, 779-791, 2003.
771 Stehfest, E., and Bouwman, L.: N_2O and NO emission from agricultural fields and
772 soils under natural vegetation: summarizing available measurement data and
773 modeling of global annual emissions, Nutrient Cycling in Agroecosystems, 74,
774 207-228, 2006.
775 Tang, X. L., Liu, S. G., Zhou, G. Y., Zhang, D. Q., and Zhou, C. Y.: Soil-atmospheric
776 exchange of CO_2, CH_4, and N_2O in three subtropical forest ecosystems in
777 southern China, Global Change Biology, 12, 546-560, 2006.
778 Van der Gon HD, Bleeker A. 2005. Indirect N2O emission due to atmospheric N
779 deposition for the Netherlands. Atmospheric Environment 39: 5827-5838.
780 Venterea, R. T., Spokas, K. A., and Baker, J. M.: Accuracy and Precision Analysis of
781 Chamber-Based Nitrous Oxide Gas Flux Estimates, Soil Science Society of
782 America Journal, 73, 1087-1093, 12009.
783 Weier, K. L., Doran, J. W., Power, J. F., and Walters, D. T.: Denitrification and
784 dinitrogen nitrous-oxide ratio as affected by soil-water, available carbon and
785 nitrate, Soil Science Society of America Journal, 57, 66-72, 1993.
786 Werner, C., Butterbach-Bahl, K., Haas, E., Hickler, T., and Kiese, R.: A global
787 inventory of N2O emissions from tropical rainforest soils using a detailed
788 biogeochemical model, Global Biogeochemical Cycles, 21, 2007a.
789 Werner, C., Kiese, R., and Butterbach-Bahl, K.: Soil-atmosphere exchange of N_2O,
790 CH_4, and CO_2 and controlling environmental factors for tropical rain forest sites
791 in western Kenya, J Geophys Res-Atmos, 112, Artn D03308, 2007b.
792 Wessen, E., Soderstrom, M., Stenberg, M., Bru, D., Hellman, M., Welsh, A.,
793 Thomsen, F., Klemedtson, L., Philippot, L., and Hallin, S.: Spatial distribution of
794 ammonia-oxidizing bacteria and archaea across a 44-hectare farm related to
795 ecosystem functioning, Isme J, 5, 1213-1225, 2011.
796 WMO: The state of greenhouse gases in the atmosphere using global observations
797 through 2008, in: Greenhouse Gas Bulletin, World Meteorological Organization,
798 4, 2009.
799 WRB: World reference base for soil resources, 2006, FAO, Rome, 3 b. pp., 2006.
800 Xiong, Z. Q., Freney, J. R., Mosier, A. R., Zhu, Z. L., Lee, Y., and Yagi, K.: Impacts
801 of population growth, changing food preferences and agricultural practices on the
802 nitrogen cycle in East Asia, Nutrient Cycling in Agroecosystems, 80, 189-198,
803 2008.
804 Zhang, W., Mo, J. M., Yu, G. R., Fang, Y. T., Li, D. J., Lu, X. K., and Wang, H.:
805 Emissions of nitrous oxide from three tropical forests in Southern China in
806 response to simulated nitrogen deposition, Plant and Soil, 306, 221-236, 2008.
807 Zhou, G. Y., Guan, L. L., Wei, X. H., Tang, X. L., Liu, S. G., Liu, J. X., Zhang, D. Q.,
808 and Yan, J. H.: Factors influencing leaf litter decomposition: an intersite
809 decomposition experiment across China, Plant and Soil, 311, 61-72, 2008.

Zhu J., Mulder J., Solheimslid S., and Dörsch P.: Functional traits of denitrification in a subtropical forest catchment in China with high atmogenic N deposition. Soil Biology & Biochemistry, Soil Biology and Biogeochemistry, 57, 577-586, 2013.

Zhu J., Mulder J., Bakken L., and Dörsch P. (submitted): The importance of denitrification in N_2O emission from N-saturated forests of SW China; results from in situ ^{15}N labeling experiments. Biogeochemistry, submitted

Table 1 Characteristics of top soils at individual plots on the hill slope (HS) and in the groundwater discharge zone (GDZ)

plot		Horizon/layer	pH (H_2O)	TOC	TN	C/N	BD[a]	$NH_4^+{}_{ex}$	$NO_3^-{}_{ex}$	$NH_4^+{}_{sw}$	$NO_3^-{}_{sw}$	IDR[b]	*Ex situ* potential of N_2O loss[b]
				mg g^{-1}			g cm^{-3}	µg N g^{-1} dw soil		mgN L^{-1}		nmol N_2O-N g^{-1} dw soil hr^{-1}	nmol NO_3^- g^{-1} dw soil
HS	T1	O	3.96	226.1	8.7	26.1	-	49.6 (20.2)	37.9 (14.7)	-	-	8.4	523
		A	3.78	10.7	0.5	20.4	0.78 (0.05)	21.5 (8.6)	59.6 (29.2)	0.11 (0.05)	15.7 (3.1)	12.2	552
	T2	O	3.74	354.5	15.7	22.6	-	81.9 (11.7)	23.7 (39.4)	-	-	16.7	2336
		A	3.84	15.0	0.8	19.4	0.72 (0.03)	34.4 (11.9)	12.7 (19.2)	0.75 (0.50)	14.9 (4.6)	13.3	1056
	T3	O	4.07	220.2	9.9	22.2	-	85.9 (19.6)	35.7 (25.1)	-	-	40.4	1924
		A	4.13	12.1	0.6	19.1	0.73 (0.15)	59.6 (30.1)	20.1 (11.2)	0.15 (0.04)	13.3 (2.8)	31.4	1624
	T4	O	3.74	326.0	13.4	24.3	-	89.2 (16.6)	29.1 (14.2)	-	-	6.4	460
		A	3.76	14.3	0.7	20.6	0.47 (0.03)	32.1 (11.6)	13.0 (4.7)	0.07 (0.02)	13.5 (4.1)	16.3	1556
	T5	O	3.67	218.1	10.1	21.6	-	55.3 (19.4)	33.6 (43.6)	-	-	26.5	1706
		A	3.75	6.5	0.4	17.2	0.76 (0.16)	25.8 (6.7)	17.4 (6.5)	0.07 (0.02)	13.4 (1.7)	14.7	1394
	B1	O	3.99	234.9	11.1	21.1	-	83.0 (16.6)	25.6 (2.9)	-	-	40.8	1236
		A	4.02	6.05	0.3	17.6	0.42 (0.07)	23.3 (5.8)	6.6 (2.3)	0.17 (0.07)	13.8 (1.5)	11.3	1014
GDZ[a]	B2	0-20 cm	4.46	14.5	0.9	15.6	1.57 (0.09)	3.6 (1.3)	6.3 (1.1)	1.25 (1.31)	6.2 (0.5)	1.8	318
	B3		4.31	12.8	0.7	18.6	1.67 (0.13)	2.8 (0.8)	2.6 (1.5)	0.01 (0.01)	1.5 (0.7)	12.3	494
	B4		4.38	23.1	1.6	14.5	0.69 (0.02)	7.9 (1.8)	1.6 (0.5)	0.02 (0.01)	5.4 (0.5)	21.0	53
	B5		4.42	11.8	0.8	14.4	0.63 (0.08)	2.9 (1.0)	2.4 (0.5)	0.02 (0.01)	0.7 (0.4)	20.1	201
	B6		4.80	40.5	2.8	14.7	1.01 (0.13)	4.3 (0.4)	0.6 (0.5)	1.12 (0.16)	0.2 (0.0)	28.0	357

TOC: total organic carbon; TN: total nitrogen; C/N: ratio of TOC and TN; BD: bulk density; $NH_4^+{}_{ex}$ and $NO_3^-{}_{ex}$: average 2M KCl-extractable $NH_4^+$and NO_3^- ; $NH_4^+{}_{sw}$ and $NO_3^-{}_{sw}$: dissolved NH_4^+ and NO_3^- in soil water and groundwater in summer 2010 (May 11 – Sep. 26, 2010); IDR: instantaneous denitrification rate in anoxic soil slurries with ample NO_3^-; *Ex situ* potential of N_2O loss: nmol NO_3^- g^{-1} dw soil denitrified before maximum N_2O reduction to N_2 was observed in anoxic soil slurries with ample supply of NO_3^-. Data in parentheses are the standard error.

[a] data from Sørbotten (2011) obtained using 100 cm^3 steel cylinders in three replicates for A horizon for each sampling plot.

[b] data from Zhu et al. (2013)

Figure 1 Location of the Tieshanping (TSP) forest catchment, Chongqing, China (panel a) and plot layout in the TSP catchment (panel b). Plots T1 to T5 constitute transect T on the hill slope (HS); Plots B1 to B6 constitute transect B in the ground water discharge zone (GDZ). Increasing plot number denote decreasing elevation along the transects. Plots T5 and B1 are at the intersection of HS and GDZ.

Figure 2 Daily average air temperature and daily precipitation at TSP. The temperature data from Sep. 5 to Sep. 18, 2009, Nov. 29, 2009 to Jan. 16, 2010 and Jan. 29 to Feb. 8, 2010 were missing. Shaded area indicates the dry-cool season.

Figure 3 Soil water filled pore space (WFPS, panel a) and soil temperature (ST, panel b) at 10 cm depth at plots T3 and B1. Shaded area indicates the dry-cool season.

Figure 4 Groundwater level (GWL) in GDZ. The lower panel indicates plots and dates at which the groundwater level was below the bottom of the monitoring well. Shaded area indicates the dry-cool season.

Figure 5 Mean N_2O flux (n=3) at the plots on the hill slope (HS, panel a) and in the ground water discharge zone (GDZ, panel b). Standard errors are not shown to maintain readability of the figure. Shaded area indicates the dry-cool season.

728 Figure 6 Cumulative N_2O fluxes (g N_2O-N m^{-2}) during summer 2009 (panel a, from
729 Jul. 12 to Aug. 8, 27 days) and 2010 (panel b, from May 10 to Aug. 24, 106 days) at
730 individual plots (n=3). Error bars represent standard error.

731

732 Figure 7 NO_3^- concentration (mg N L^{-1}) in soil pore water at 5 cm depth at each plot
733 of HS (panel a) and of groundwater at 30 cm depth in GDZ (panel b), respectively.
734 NO_3^- values from some of the HS plots during summer 2009 are missing because
735 samplers were damaged by worms. Shaded area indicates the dry-cool season.

736

737 Figure 8 Principal component analysis of cumulative N_2O fluxes and soil parameters
738 (Table 1) at TSP. Before analysis, the N_2O flux and several of the parameters were
739 transformed, whereas others (TOC: total organic carbon; TN: total nitrogen; C/N: the
740 ratio of TOC and TN; IDR: instantaneous denitrification rate; *ex situ* potential of N_2O
741 loss (see text for explanation); $NH_4^+{}_{ex}$ and $NO_3^-{}_{ex}$: 2M KCl -extractable NH_4^+ and
742 NO_3^-) were not. The transformations were as follows: N_2O flux: ln(cumulative N_2O
743 flux from each plot in summer 2010; Fig. 6); bulk density (BD): -1/(bulk density);
744 $NH_4^+{}_{sw}$: ln(dissolved NH_4^+) in soil water; $NO_3^-{}_{sw}$: sin(dissolved NO_3^- in soil water).
745 Red points indicate the individual plots.

746

747 Figure 9 Observed and simulated average N_2O flux at hill slope (HS). The shaded area
748 denotes the dry-cool season.

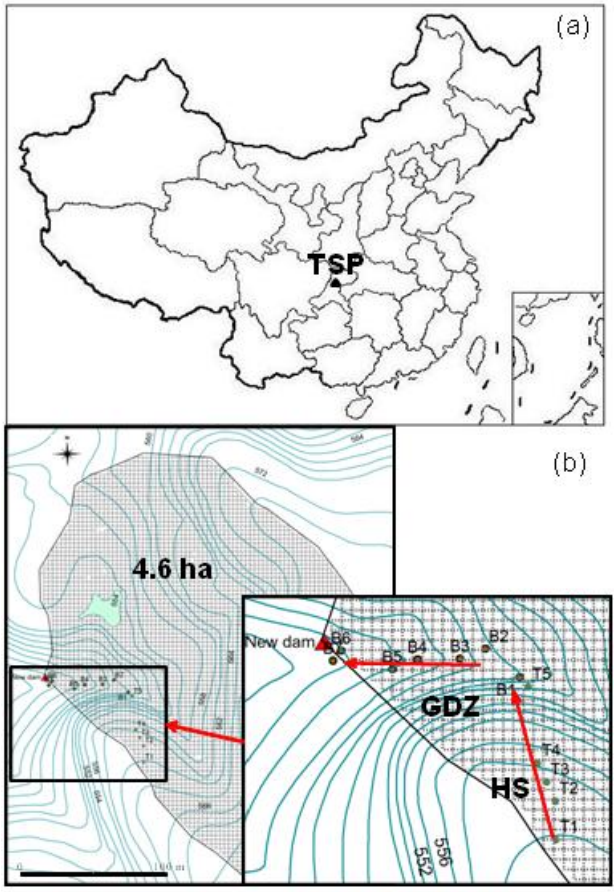

749

750

751 Fig. 1

752

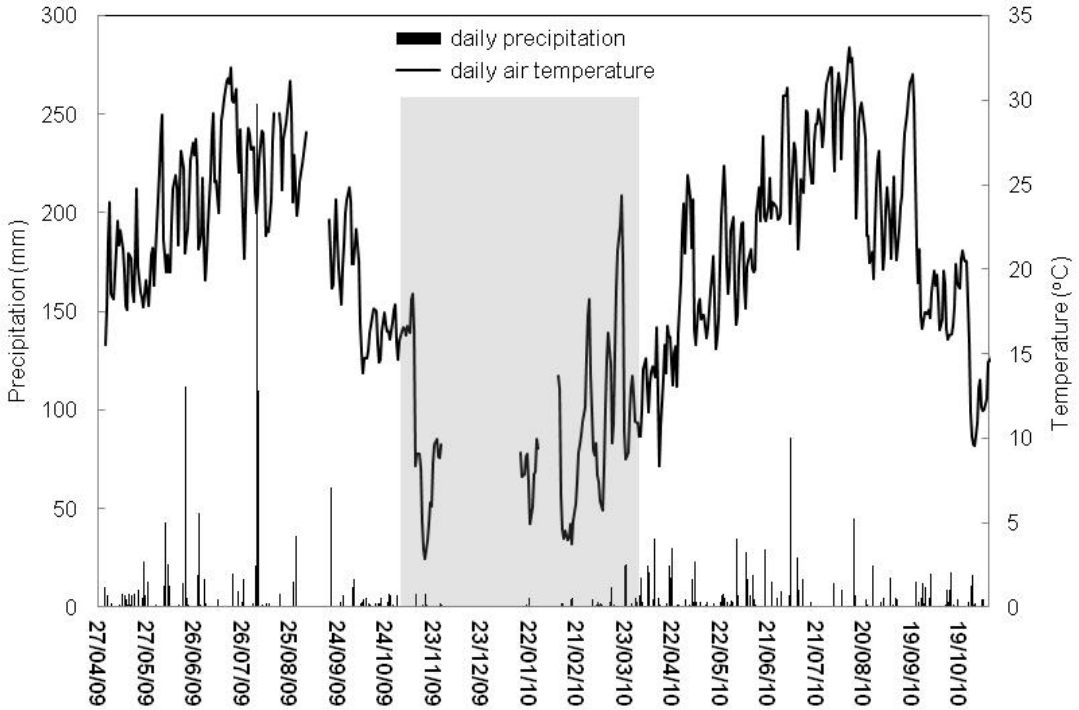

753

754

755 Fig. 2

756

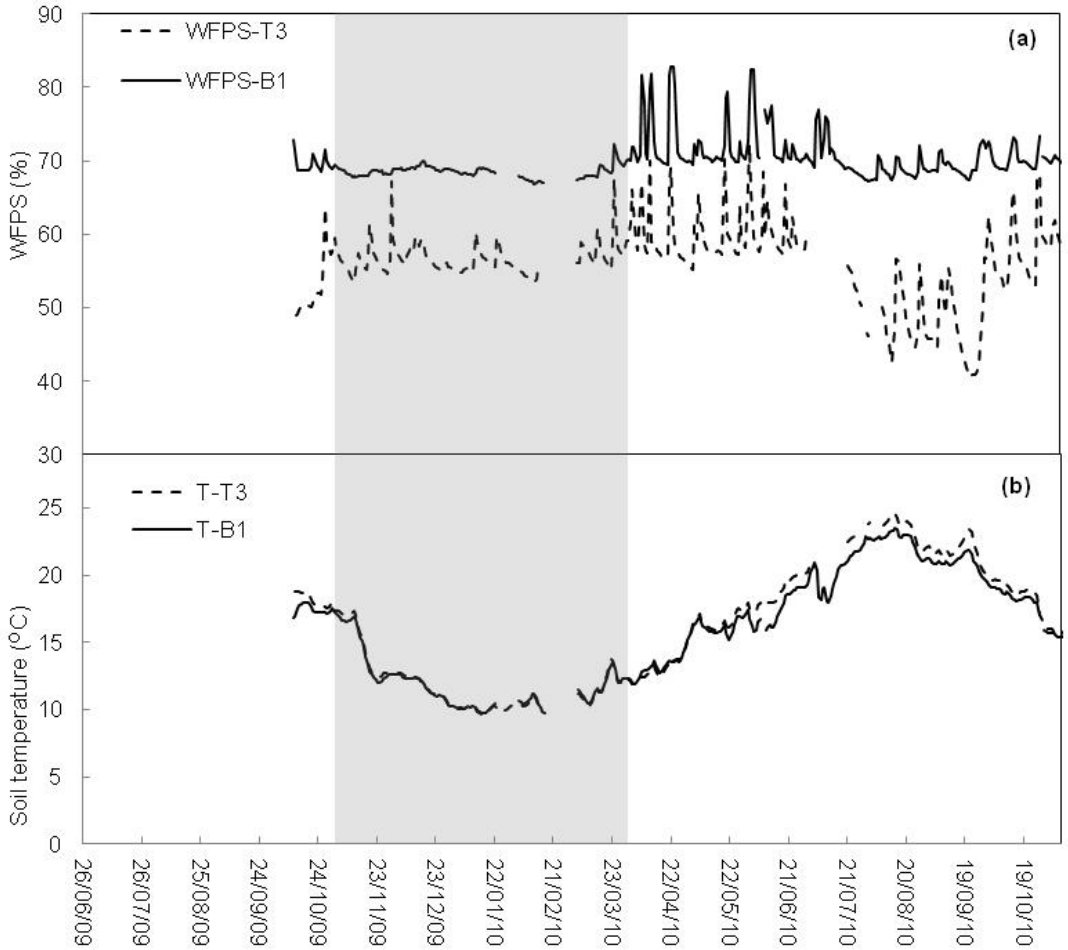

757

758

759 Fig. 3

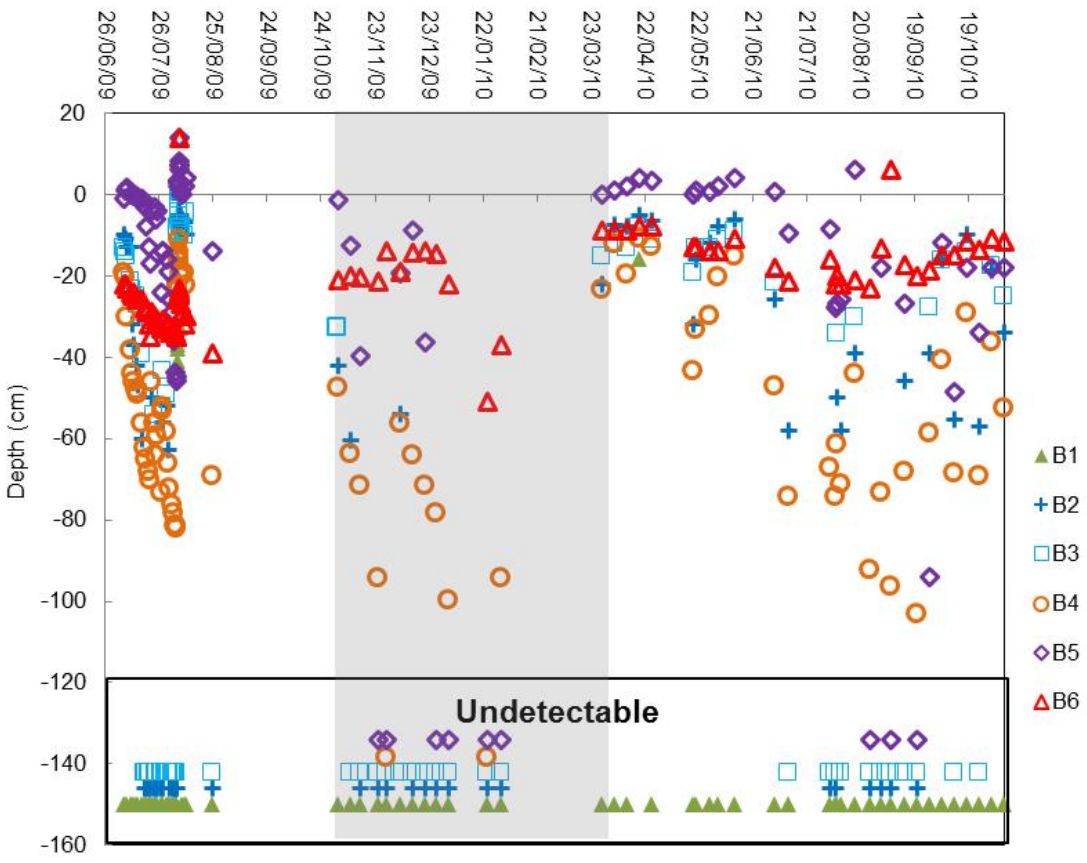

760

761

762 Fig. 4

763

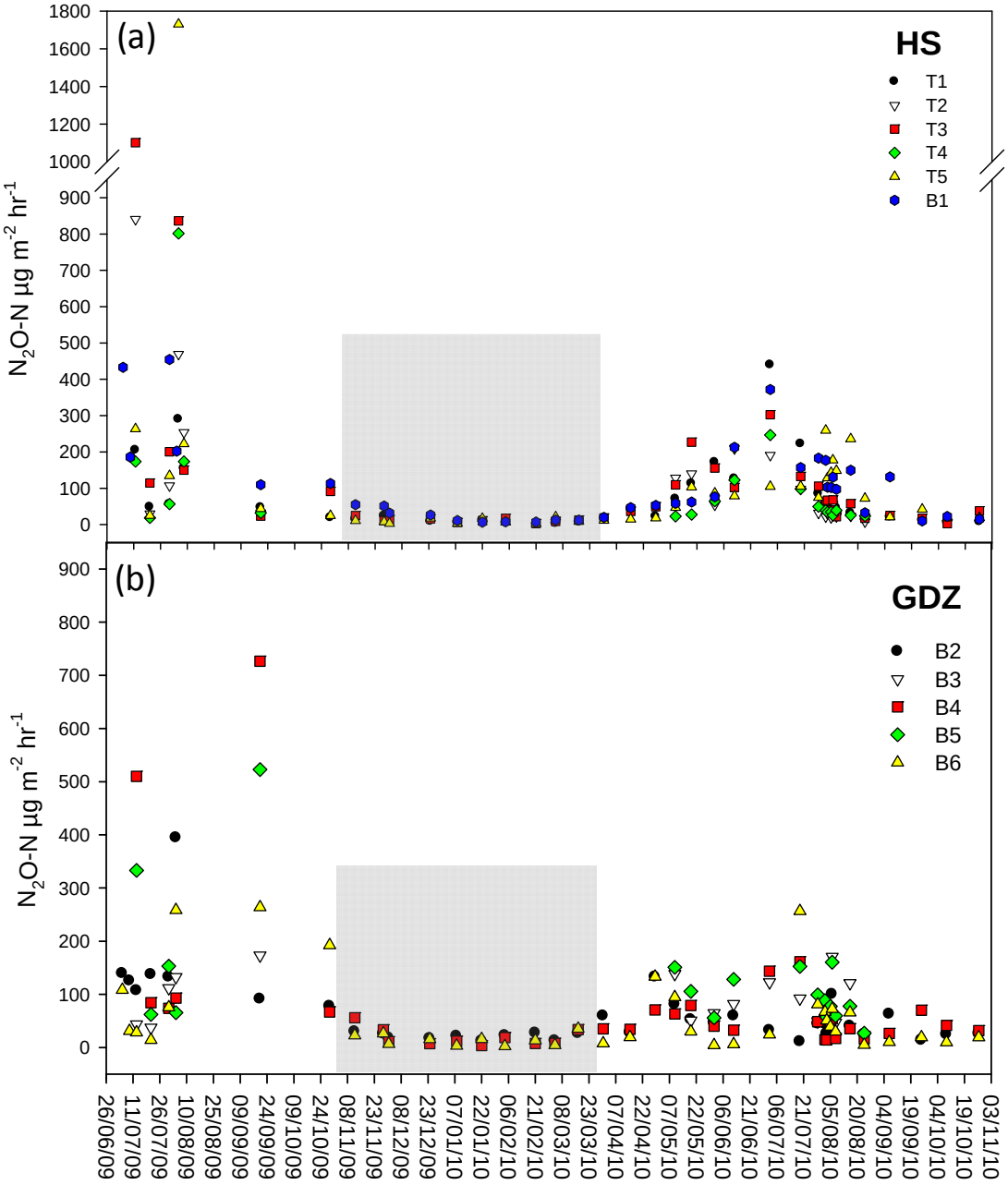

764

765

766 Fig. 5

767

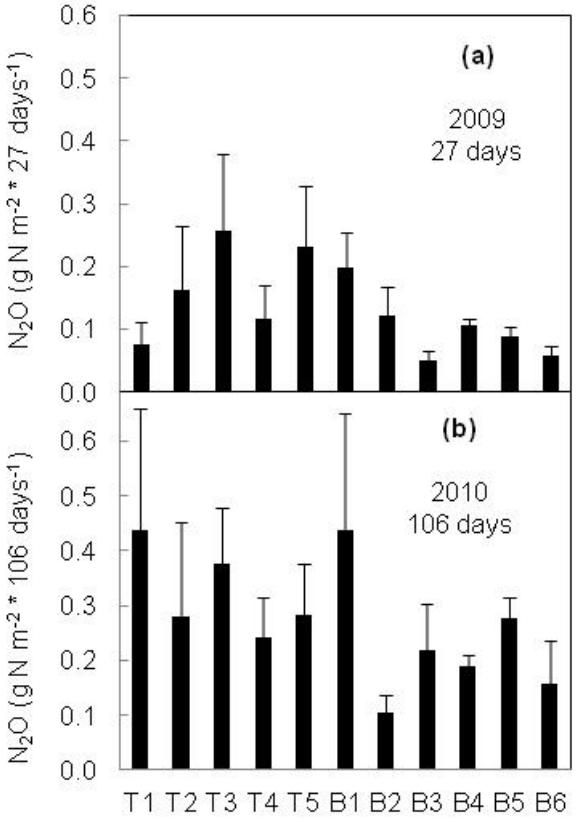

768

769

770 Fig. 6

771

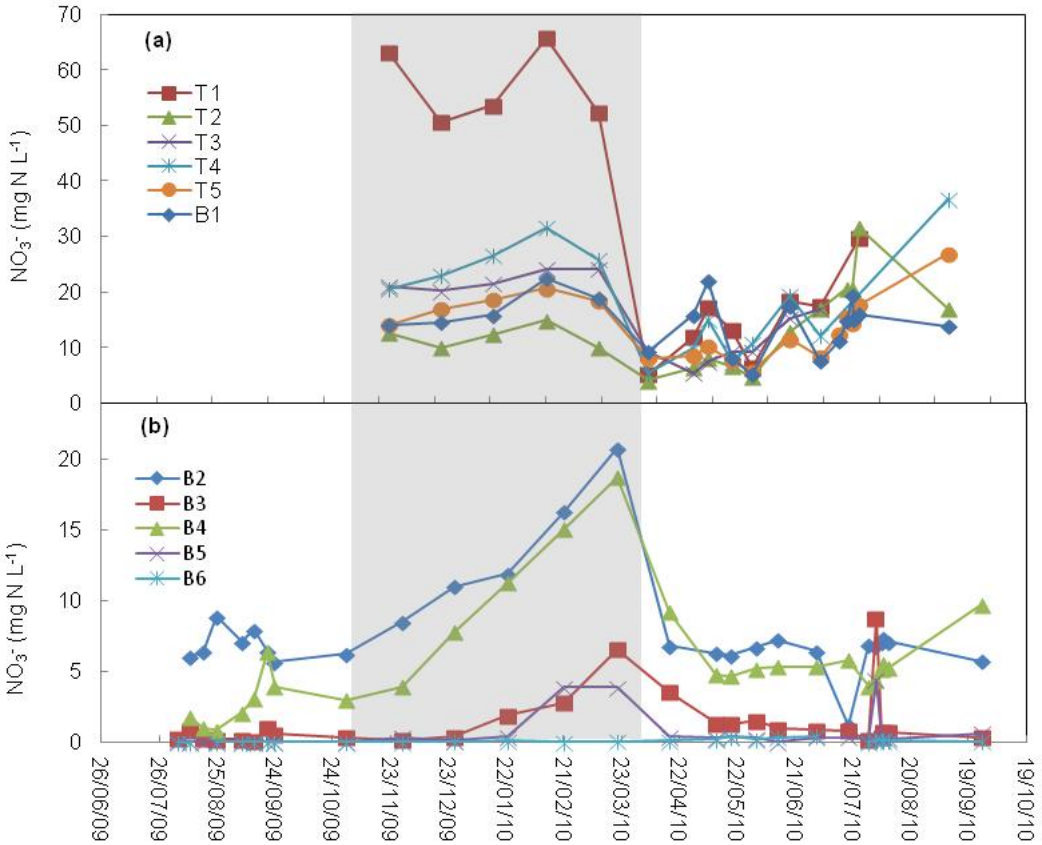

772

773

774 Fig. 7

775

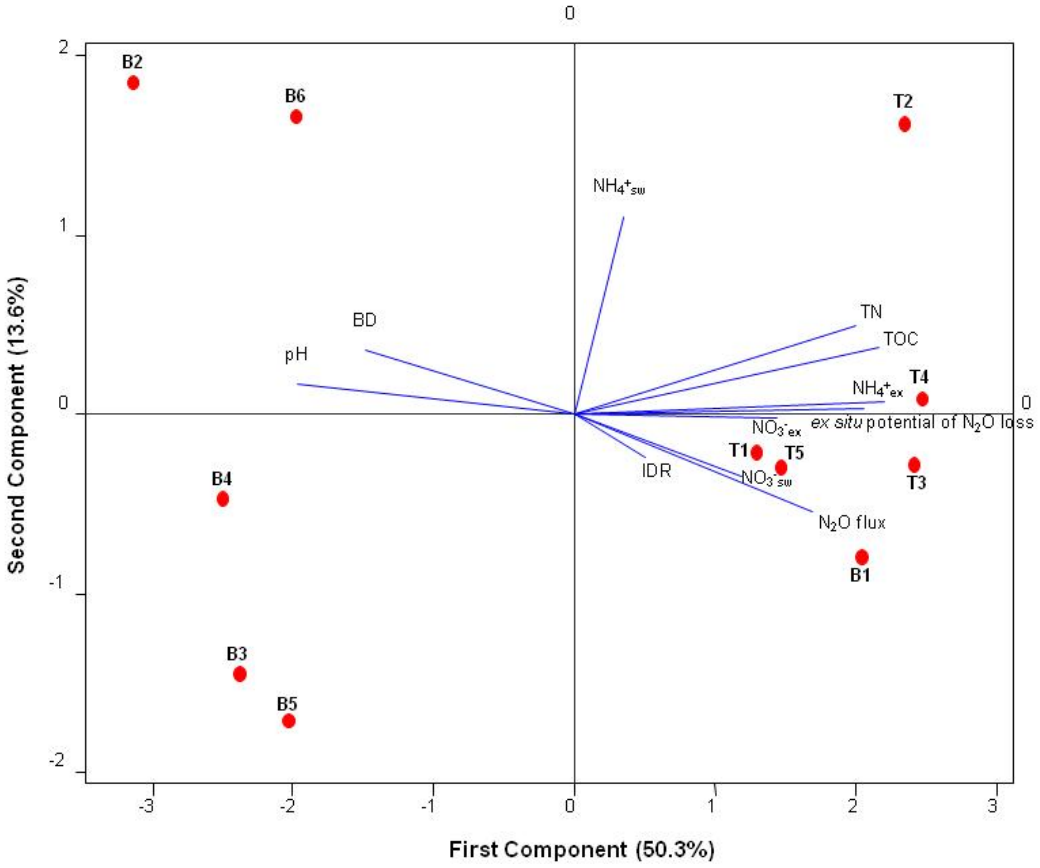

776

777

778 Fig. 8

779

780

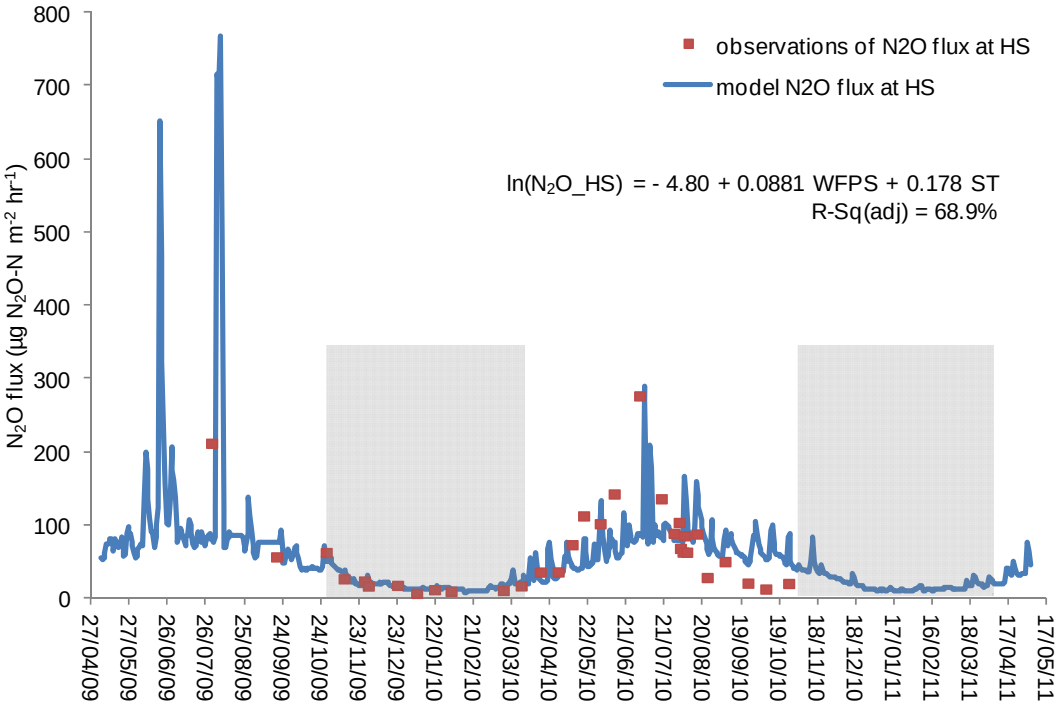

781

782 Fig. 9

783